Hindawi
Shock and Vibration
Volume 2022, Article ID 5404908, 13 pages
https://doi.org/10.1155/2022/5404908

Research Article

Seismic Response and Damage Analysis of Large Inverted Siphon Structure

Yanke Shi,[1,2] **Lin Xu**,[2] **Rongbin Hou**,[1,2] **Dekang Zhang**,[2] **and Duoxin Zhang**[2]

[1]*MWR Center for Levee Safety and Disease Prevention Research, Yellow River Institute of Hydraulic Research, Zhengzhou 450003, China*
[2]*School of Civil Engineering and Communications, North China University of Water Resources and Electric Power, Zhengzhou 450045, China*

Correspondence should be addressed to Duoxin Zhang; dxzhang@ncwu.edu.cn

Received 31 March 2022; Revised 28 April 2022; Accepted 16 May 2022; Published 24 June 2022

Academic Editor: Honglue Qu

Large-scale inverted siphon is a key hydraulic structure for building a national water network and realizing the spatial balance of water resources, and its safety under the action of earthquakes has become the focus of trans-basin water transfer projects. In this paper, Xiazhuang inverted siphon of water diversion in Central Yunnan is taken as the research object. Viscoelastic artificial boundary was used to simulate seismic waves spread in the soil, which include the natural site seismic waves and the waves fitted manually according to the site conditions. A three-dimensional finite element model of soil-structure-fluid interaction was established by software of ABAQUS, in which the fluid-structure interaction was simulated by user-defined element (UEL) built on additional Mass Method. Seismic response and damage analysis of large inverted siphon structure are carried out by the model. The results show that the dynamic displacement of the inverted siphon pipe is mainly horizontal sloshing, and the dynamic response of the pipe increases due to the water in the pipe; even the dynamic stress value in some areas is close to the design value of the concrete tensile strength. The damage analysis of inverted siphon pipe shows that the plastic deformation and the damage area develop rapidly with the increase of the peak ground acceleration (PGA), and the tensile damage area is generally larger than the compression damage area. The damage factor of the pipe under the working condition of the water is obviously larger relative to the working condition of no water. Therefore, it is suggested that the damage effect of earthquake should be considered in the design of large inverted siphon in high-intensity area.

1. Introduction

Large-scale inverted siphon is a key hydraulic structure for building a national water network and realizing the spatial balance of water resources. In the cross-basin water transfer projects that have been built or planned, the scale of inverted siphon tends to be large or giant, and its response under earthquake action is a concern problem in the engineering and technical field. As the inverted siphon is usually a special-shaped structure with 2–3 holes combined in one section, the responses of deformation and stress are very complex under various loads during the construction and operation period. Scholars have carried out a series of studies and achieved some valuable scientific research results. However, there are relatively few research achievements considering the interaction between the pipe and the soil, the fluid-solid coupling between the water and the structure, and the damage mechanism of the pipe body under the action of earthquake.

In China's South-to-North Water Diversion Project, Zhao et al. [1] carried out an inverted siphon model test study and compared it with the finite element results; Liu et al. [2] studied temperature control and crack prevention measures of the circular-hole-square inverted siphon during

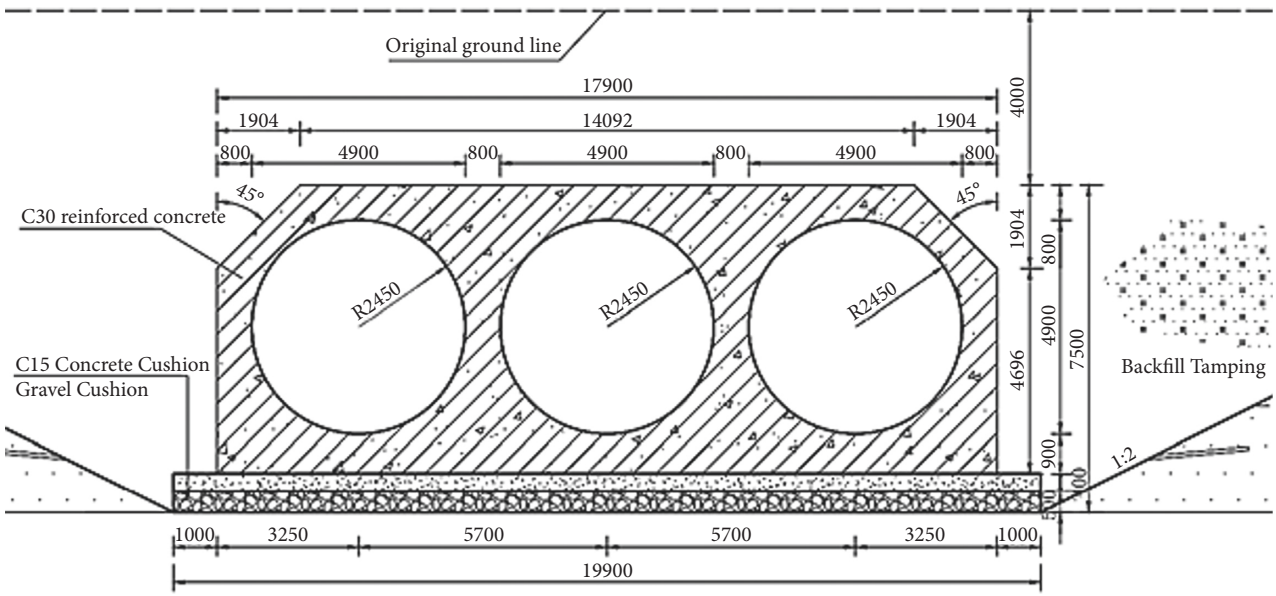

Figure 1: The cross section of inverted siphon structure (unit: mm).

the construction period; Shi et al. [3] conducted a study on reasonable pipe length of inverted siphon. Unfortunately, the earthquake effect was not considered in these previous studies.

Wang et al. [4, 5] took the inverted siphon of Nansha river as the research object and analyzed the dynamic response of the inverted siphon under different working conditions; however, they did not consider the interaction between pipes and soil; Xu et al. [6] carried out the dynamic response analysis of Xiaqin River inverted siphon under the excitation of bidirectional seismic waves, but they did not consider the influence of water in the pipe; Ai and Li [7], taking into account the joint action of soil and groundwater around the pipeline, adopted the nonlinear material constitutive model and analyzed the dynamic response of the underground pipeline through the effective stress method; Fu and Gu [8] used two-dimensional uniform equivalent viscoelastic artificial boundary conditions to summarize the response law of highway mountain tunnel under earthquake action; Han et al. [9] analyzed the seismic response of the subway station under the action of near- and far-site seismic waves based on ABAQUS and gave the location of subway station vulnerable to damage under the action of earthquake. Qu et al. [10, 11] developed an analytical model in modeling the dynamic responses of the pile, anchor cable, and soil slope system based on Winkler elastic foundation beam theory. Although the research objects of literature [7–11] are pipeline structure, tunnel structure, subway, and pile wall structure, they provide ideas for the author's research.

In this paper, the viscoelastic artificial boundary was used to simulate the input of seismic waves, which include the natural site seismic waves and the waves fitted manually according to the site conditions. Seismic response and damage analysis of large inverted siphon structure are carried out by the three-dimensional finite element model of soil-structure-fluid interaction established by the software of ABAQUS, in which the fluid-structure interaction was simulated by user-defined element (UEL) built on additional Mass Method.

2. Research Object

Xiazhuang inverted siphon is one of the important structures of the Central Yunnan Water Diversion Project, which is the largest scale and the most investment water project in southwest China. The inverted siphon was buried underground, which is made of 3 reinforced concrete pipes combined in one section with a diameter of 4.9 m. In this paper, the standard section, which accounts for 68% of the total length of the inverted siphon, is selected as the research object. The thickness of the bottom plate is 0.9 m, the thickness of the side wall and the top arch is 0.8 m, the head of the internal water is 15 m, and the buried depth is 4 m; the pipes is made of C30 concrete, the stressed steel bar is HRB400, and the bottom cushion of the inverted siphon is made of C15 concrete; the foundation is mainly clay layer and no foundation treatment. The cross section of the inverted siphon structure is shown in Figure 1.

3. Calculation Model and Analysis Conditions

3.1. Calculation Model. Considering the influence of the boundary effect of the foundation soil, the soil on both sides was selected to be twice the width of the siphon from the side wall and four times the height of the pipe from the bottom of the foundation depth. The z direction of the model is the vertical direction, X is the horizontal direction, and Y is the water delivery direction. The bottom boundary of the foundation is fixed, the top surface of the backfill is free boundary, and other model boundaries are normal constraints. The finite element model established by the software of ABAQUS is shown in Figure 2.

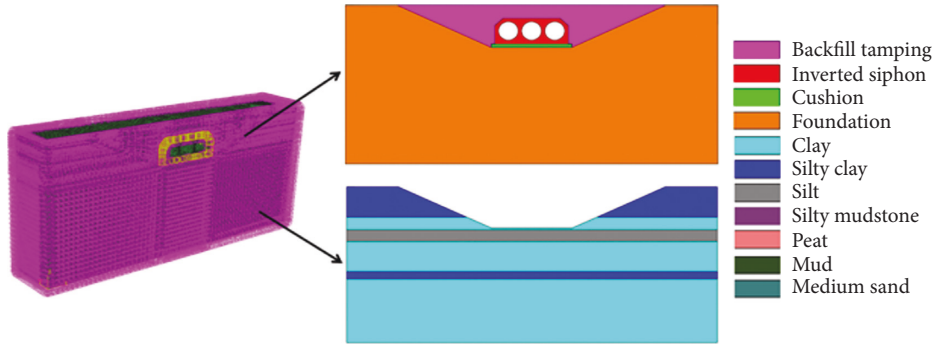

Figure 2: Finite element model.

Table 1: Mechanical parameters of materials.

Category	Gravity (kg/m³)	Elasticity modulus (MPa)	Poisson's ratio	Cohesion (kPa)	Internal friction angle (°)
Inverted siphon	2500	31000	0.2		
Plain concrete cushion	2400	22000	0.167		
Gravel cushion	2700	30000	0.2		
Rubber water stop	800	7.8	0.47		
Back fill	2000	30	0.35	4.00	30
Silty clay	1900	30	0.3	18.40	16
Silt	2000	40	0.3	22.50	14
Medium fine sand	2000	75	0.25	0	30
Clay	2200	35	0.35	23.90	16

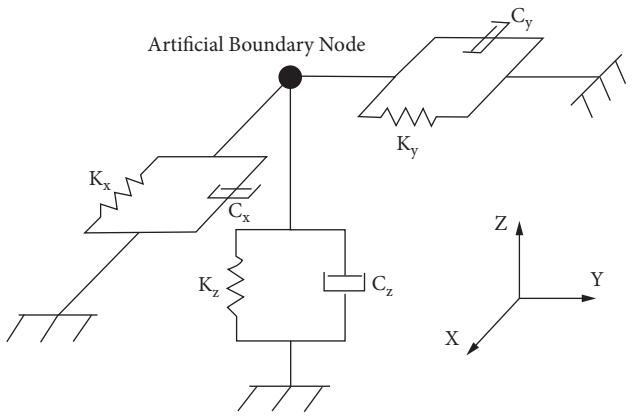

Figure 3: Schematic of 3D viscoelastic artificial boundary model.

3.2. Parameters of Material and Contact Properties. The material parameters of the finite element model are selected according to the engineering as shown in Table 1. The soil is simulated by Mohr–Coulomb model. Due to the complexity of reinforcement of inverted siphon, the equivalent elastic modulus of reinforced concrete pipe is calculated according to the principle of stiffness equivalence, which can be calculated as follows:

$$\overline{E}_R = E_C\left(1 + \rho\frac{E_S - E_C}{E_C}\right), \tag{1}$$

where $\overline{E}_R$ is the equivalent elastic modulus of reinforced concrete, E_C is the elastic modulus of concrete, E_S is the elastic modulus of steel, and ρ is the reinforcement ratio.

The concrete and soil are simulated by solid element (C3D8R), the viscoelastic artificial boundary was used for

Table 2: The formulas for calculating spring stiffness and damping coefficient.

K_{BN}	K_{BT}	C_{BN}	C_{BT}
$\alpha_N G/R$	$\alpha_T G/R$	ρc_p	ρc_s

K_{BN}, K_{BT}, C_{BN}, and C_{BT} are the normal and tangential spring stiffness and damping coefficients of the viscoelastic artificial boundary. E is the elastic modulus of foundation. G is the shear modulus of foundation. ρ is the density of the foundation. R is the distance from the scattered wave source to the artificial boundary, and the scattering source is taken as the geometric center of the underground structure. α_N, α_T, A, and B are calculation parameters, and the recommended values are 1.33, 0.67, 0.9, and 1.1, respectively.

dynamic boundary conditions, and the user-defined additional mass element was used to simulate water inside the pipe. Tie contact was defined between pipe and cushion, hard contact was defined between pipe and soil in the normal direction, and friction contact was defined in the tangential direction. The friction coefficient was set as 0.4, and elastic slip behavior between contacts was considered.

The fluid-structure interaction was simulated by user-defined element (UEL) built on additional Mass Method. The hydrodynamic pressure in the pipe is converted into the radial additional mass of the pipe wall corresponding to the unit seismic acceleration, which can be calculated as follows:

$$M_l = \frac{7}{8}A_l\rho\eta\sqrt{H_0 h}, \tag{2}$$

where M_l is the additional mass at node l; A_l is the influence area at node l; ρ is the density of water; η is the reduction

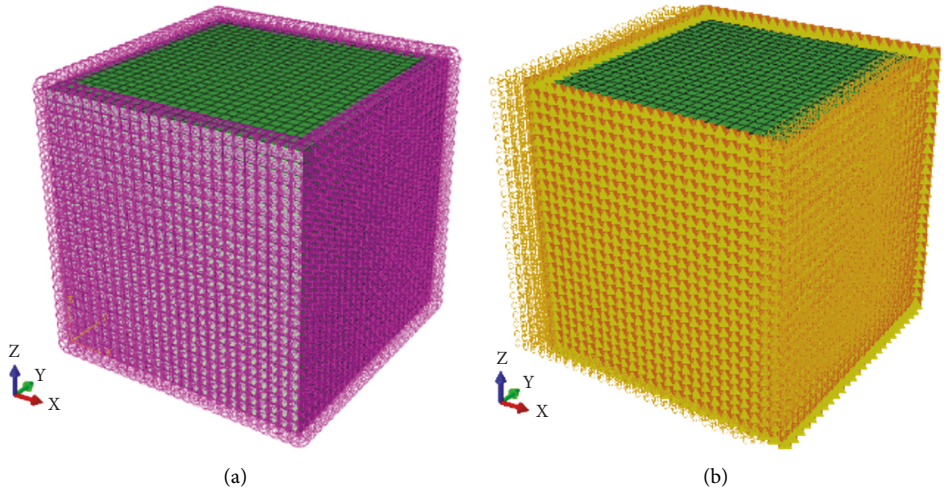

(a) (b)

Figure 4: Viscoelastic artificial boundary finite element model with implicit and explicit solver. (a) Implicit algorithm; (b) explicit algorithm.

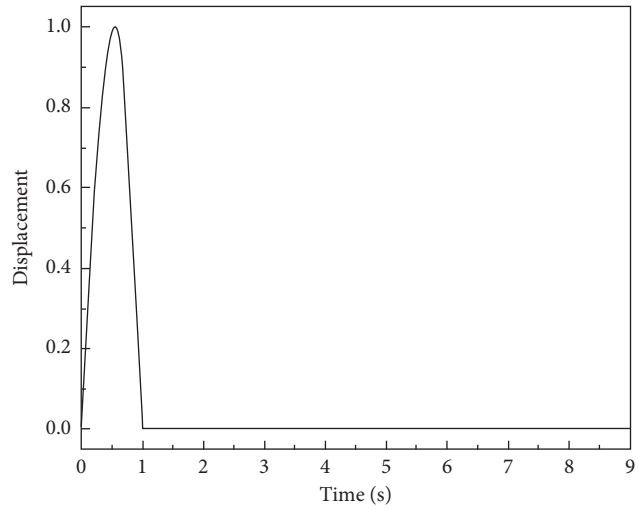

Figure 5: Pulse wave displacement time-history curve.

factor, which is taken as 1 in the paper; H_0 is the water depth; and h is the distance from node l to water surface.

3.3. Viscoelastic Artificial Boundary. In this paper, soil-structure interaction is achieved through the viscoelastic artificial boundary, which was used to simulate seismic waves spread in the soil. The three-dimensional viscoelastic artificial boundary model is shown in Figure 3. Normal and tangential spring-dampers are provided in all three directions of the foundation boundary. Liu et al. [12] derived the in-plane normal viscoelastic artificial boundary under the action of cylindrical waves. The formulas are given in Table 2 to calculate the spring and damping parameters of artificial boundary conditions based on the research results of Liu Jingbo. The normal and tangential viscoelastic artificial boundary conditions are realized by finite element software simulation on basis of the content. C_P and C_S are p-wave velocities and s-wave velocities in foundation media, which can be calculated as follows:

$$C_P = \sqrt{\frac{\lambda + 2\mu}{\rho}} = \sqrt{\frac{(1-\nu)E}{(1+\nu)(1-2\nu)\rho}},$$
$$\mathrm{CS} = \sqrt{\frac{\mu}{\rho}} = \sqrt{\frac{E}{2(1+\nu)\rho}}, \tag{3}$$

where λ, μ, and ν are Lame constants and Poisson's ratio.

In this paper, the interaction between soil and structure can be realized by using suitable viscoelastic artificial boundary simulation when dynamic calculations are performed for the inverted siphon structure. The soil response is calculated, respectively, using the implicit solver and the explicit solver under impulse excitation. The correctness of the three-dimensional viscoelastic human boundary absorbing reflected wave energy and the ground motion input method are verified according to the comparation with the analytical solution under ideal conditions. The verification process is as follows.

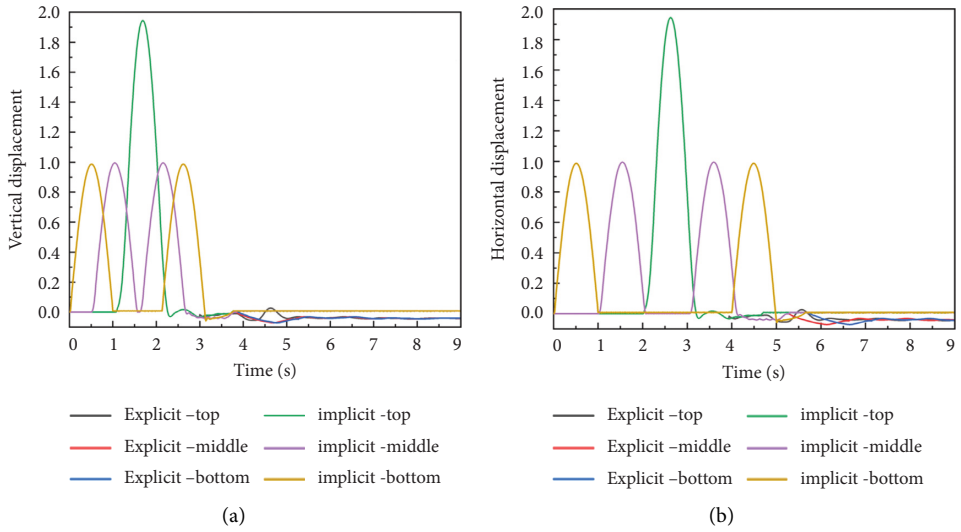

Figure 6: Displacement time-history curve. (a) Vertical displacement time-history; (b) horizontal displacement time-history.

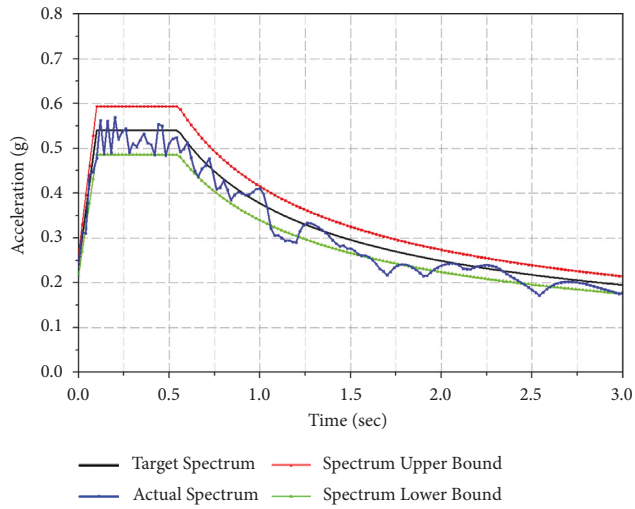

Figure 7: Response spectrum of synthetic seismic wave.

A cube soil with a side of 300 meters is taken as an example, which is simulated by the C3D8R element. Spring1 and Dashpot1 elements are used to simulate viscoelastic boundary under implicit solution condition, and connector element is used to simulate viscoelastic boundary under explicit solution condition as shown in Figure 4. The elastic modulus of soil is 117 MPa, the shear modulus is 45 MPa, the density is 2000 kg/m^3, and the Poisson's ratio is 0.3. The shear wave velocities and longitudinal wave velocities in the soil medium are obtained based on the parameters, which are c_s = 150m/s and c_p = 280.62m/s.

Two horizontal impulse shear waves and one vertical impulse compression wave are input on the artificial boundary of the soil. The displacement time-history curves of the three waves shown in Figure 5 are consistent, and the total calculation time is 9 s. The time-history curves of the top, middle, and bottom positions are calculated based on different solvers as shown in Figure 6.

As shown in Figure 6, when the soil displacement is transmitted to the free surface on the top of the soil after a certain period of time, its amplitude is amplified by nearly two times, which is basically consistent with the analytical results under ideal conditions. According to the comparison between the calculated results and the analytical solutions, it is proved that the viscoelastic boundary used by the paper to simulate the input of seismic waves is correct.

It is reflected that the wave is not reflecting, when the wave propagates to the free surface on top of the soil, and propagates to the bottom of the soil until the whole wave passes through the viscoelastic boundary. However, the displacement of the soil analyzed by the implicit solution method tends to zero, while the displacement obtained by the explicit solution method is 0.04 m (along the negative direction of z-axis). It indicates that the viscoelastic artificial boundary defined by Spring1 and Dashpot1 elements in the implicit solution mode has a better effect on absorbing

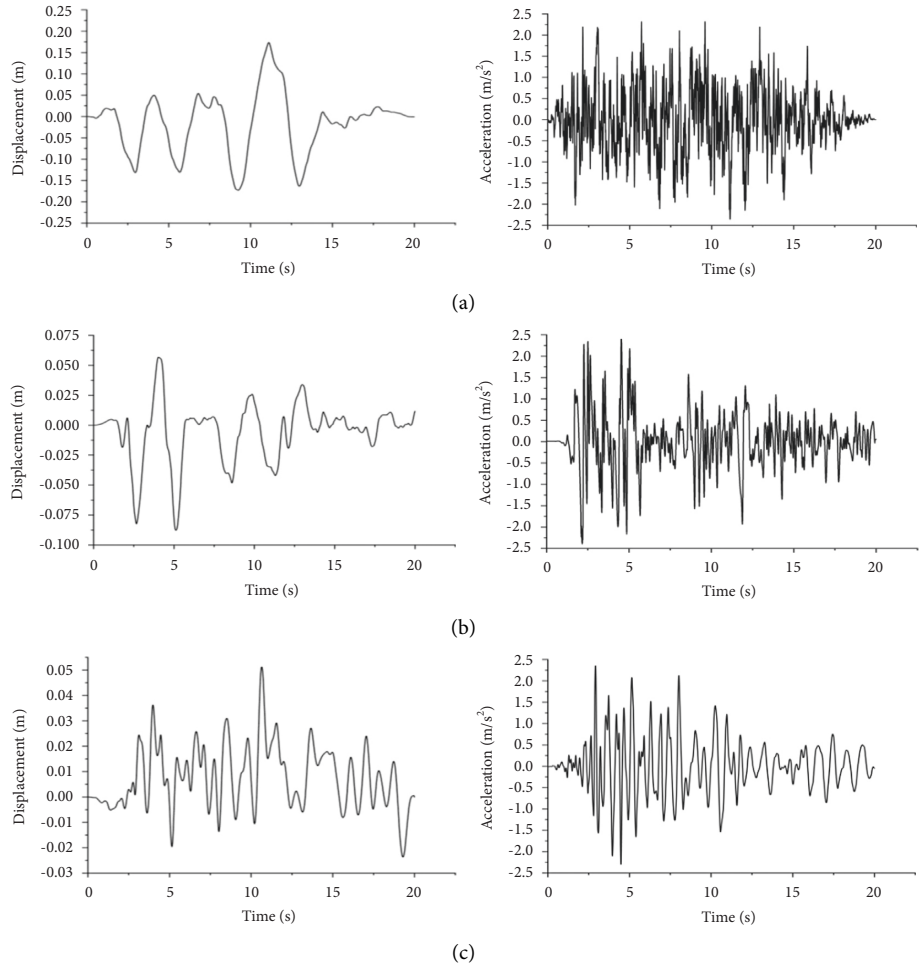

Figure 8: Acceleration and displacement time-history of earthquake ground motions. (a) Synthetic wave; (b) EL-centro wave; (c) Hollister wave.

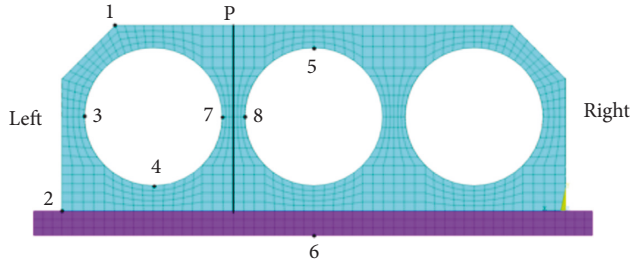

Figure 9: Distribution of characteristic points.

seismic wave energy relative to the explicit model. Therefore, the implicit solver is used to perform dynamic calculations for the inverted siphon structure.

3.4. Seismic Wave Input. According to the Ground Motion Parameter Zoning Map of China (GB18306-2015) [13] and the results of shear wave velocity test and site classification, the building site category of the research object is determined to be class III. According to the Seismic Design Standard for Hydraulic Buildings (GB5247-2018) [14], the three-way ground motion acceleration is input to the 3D model, and 2/3 of the horizontal acceleration is taken as the vertical acceleration.

According to the Seismic Safety Assessment Report of Key Engineering Sites of Water Source and Main Canal Line of Central Yunnan Water Diversion Project, the basic seismic intensity of the site of this project was 8 degrees. We adopted a peak acceleration of ground motion exceeding the probability of 10% within the reference period (the past 50 years) as the designed peak acceleration of ground motion, with an acceleration of 0.24 g, a characteristic period of

Table 3: Stress amplitude at characteristic points (unit: MPa).

Characteristic point	Synthetic wave				EL-centro wave				Hollister-02 wave			
	Without water		Water		Without water		Water		Without water		Water	
	σ_{max}	σ_{min}	σ_{max}	σ_{min}	σ_{max}	σ_{min}	σ_{max}	σ_{min}	σ_{max}	σ_{min}	σ_{max}	σ_{min}
1	1.25	−2.28	0.70	−1.12	0.64	−1.35	0.18	−1.10	0.36	−1.82	0.20	−1.11
2	0.98	−1.35	1.13	−0.51	0.88	−0.80	0.73	−0.62	0.46	−0.67	0.89	−0.65
3	1.44	−0.81	1.11	−0.68	0.50	−0.85	0.64	−0.63	0.52	−0.66	0.41	−0.92
4	0.28	−1.44	0.22	−2.01	0.25	−1.12	0.22	−1.53	0.24	−0.83	0.40	−1.30
5	0.16	−0.55	0.20	−0.92	0.13	−0.43	0.10	−0.75	0.18	−0.33	0.38	−0.92
6	0.07	−0.24	0.05	−0.50	0.09	−0.25	0.07	−0.50	0.07	−0.17	0.16	−0.52

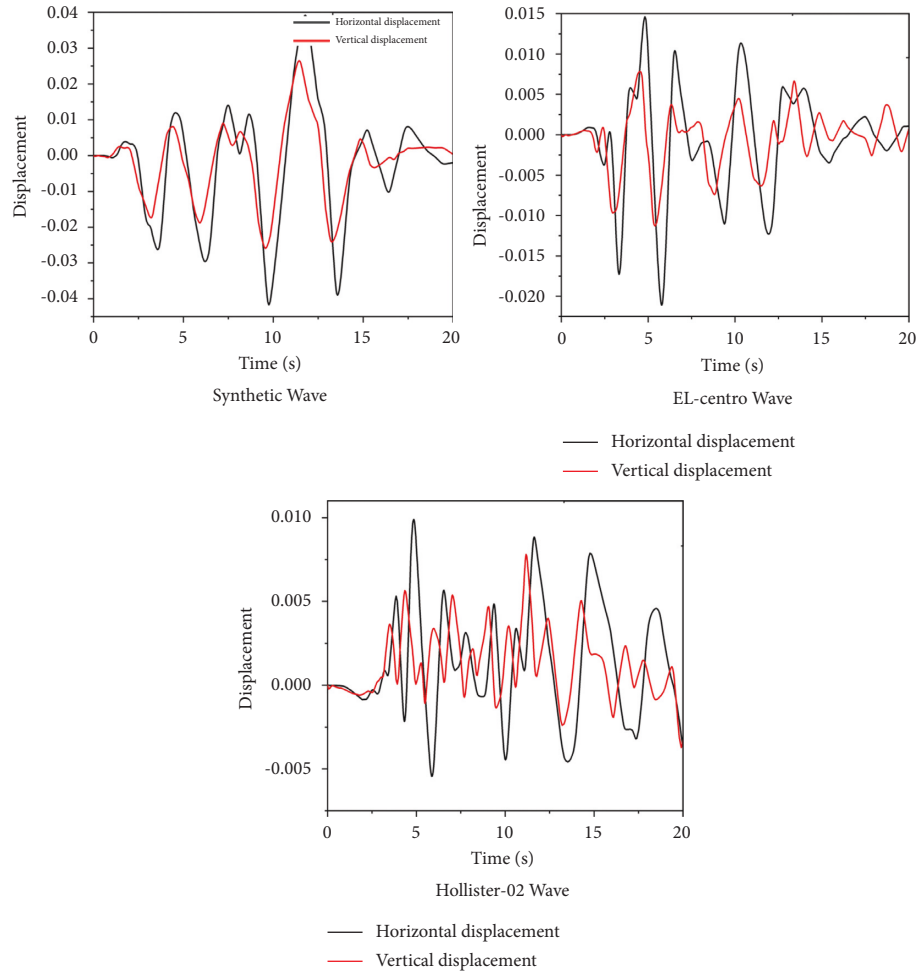

(a)

Figure 10: Continued.

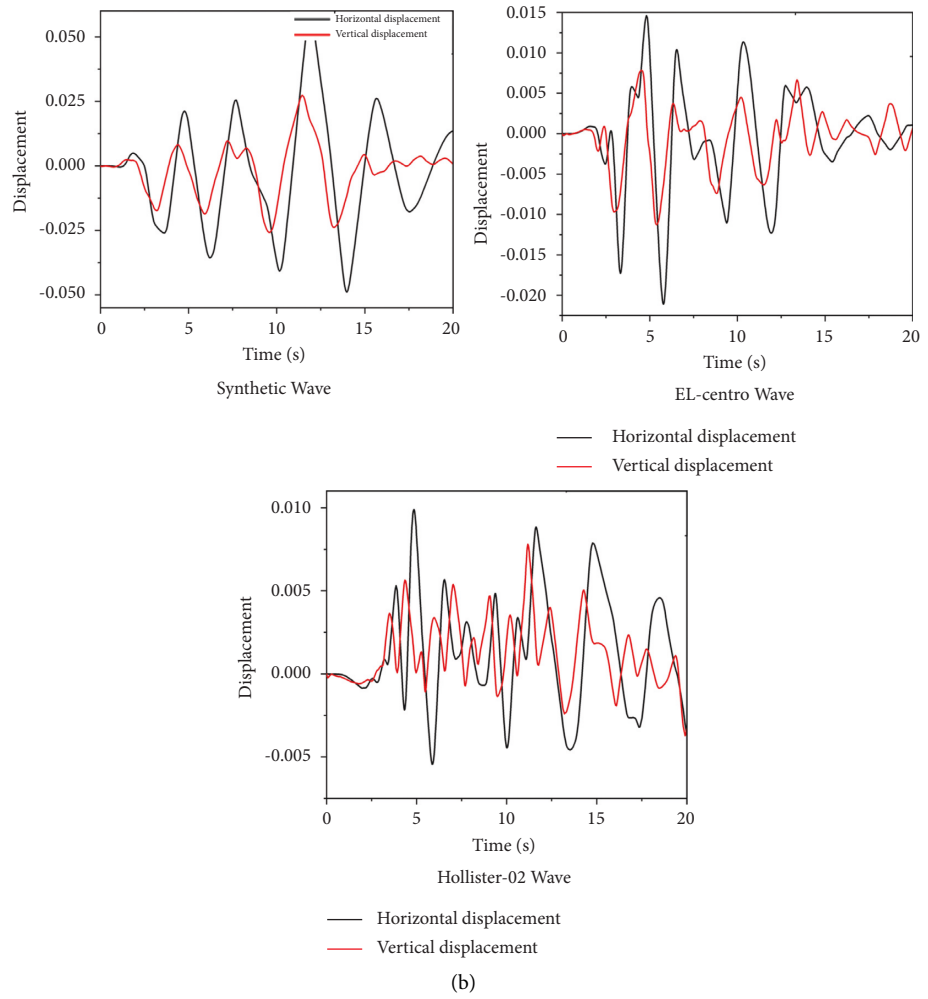

Figure 10: Displacement response time-history of the characteristic point on the top of the middle tube. (a) Empty pipe condition; (b) three pipe water filled.

Table 4: Displacement response maximum value at characteristic point 5 (unit: m).

Displacement response	Empty pipe condition			Three pipe water filled		
	Synthetic wave	EL-centro wave	Hollister-02 wave	Synthetic wave	EL-centro wave	Hollister-02 wave
Lateral displacement	0.042	0.021	0.010	0.057	0.026	0.014
Vertical displacement	0.027	0.011	0.008	0.027	0.012	0.007

0.55 s, and a damping ratio of 0.05. The target acceleration response spectrum was determined by the standard design of the hydraulic structure response spectrum [14]. The response spectrum of the synthetic seismic wave with the adoption of Fourier transforms and the Jennings envelope on the basis of target acceleration response spectrum is shown in Figure 7.

The seismic waves are input to the inverted siphon structure as shown in Figure 8.

4. Seismic Response Analysis

Three seismic waves are used to analyze the dynamic response of the Xia Zhuang inverted siphon structure based on the calculation model and calculation conditions in Section 2. The characteristic points are used to describe the properties of the inverted siphon pipes shown in Figure 9. The path taken between characteristic point 7 and characteristic point 8 is used to analyze the displacement and stress of the pipes. The principal stress amplitude at each characteristic point is shown in Table 3.

In without water condition, it can be seen that the extreme value of the first principal stress at feature point 3 is 1.44 MPa which is slightly higher than the design value of C30 concrete tensile strength. The extreme value of the first principal stress at other characteristic points is lower than the design value of concrete tensile strength, and the maximum compressive stress at all characteristic points is

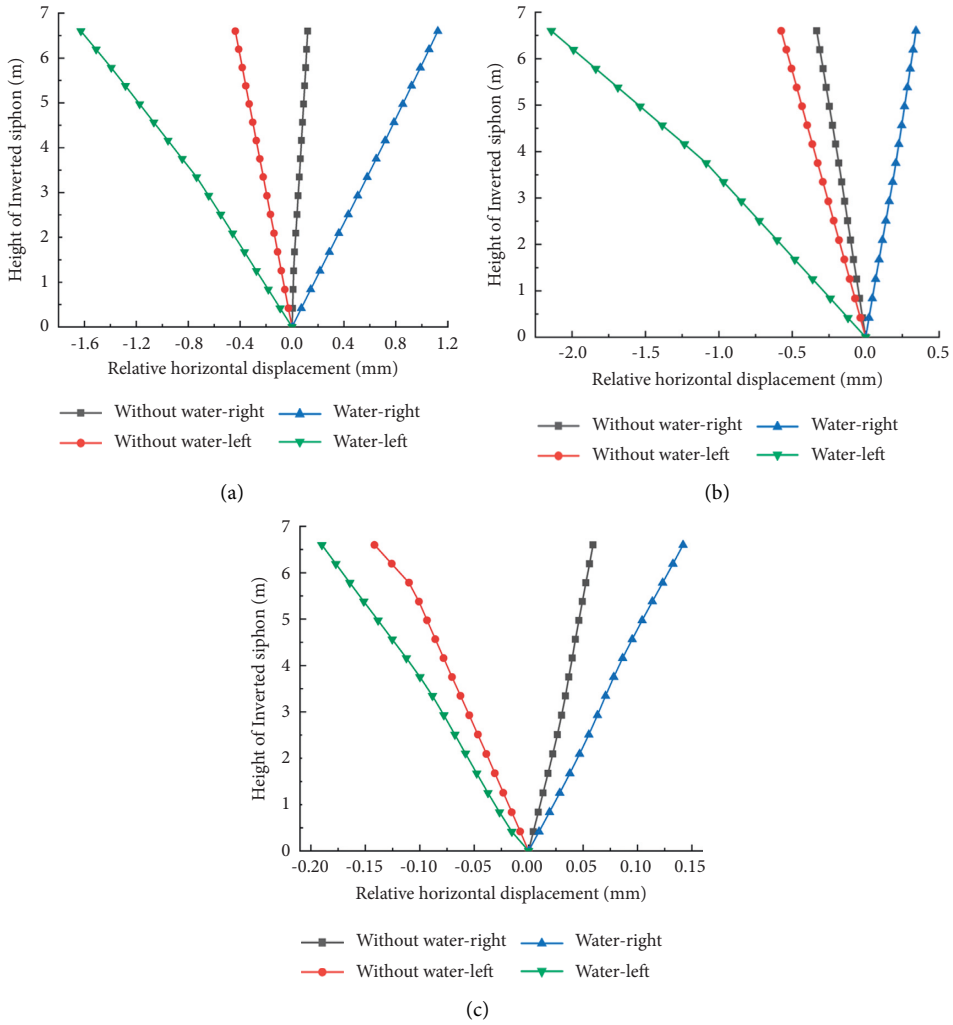

Figure 11: Variation curve of horizontal relative displacement along height. (a) Synthetic wave; (b) EL-centro wave; (c) Hollister-02 wave.

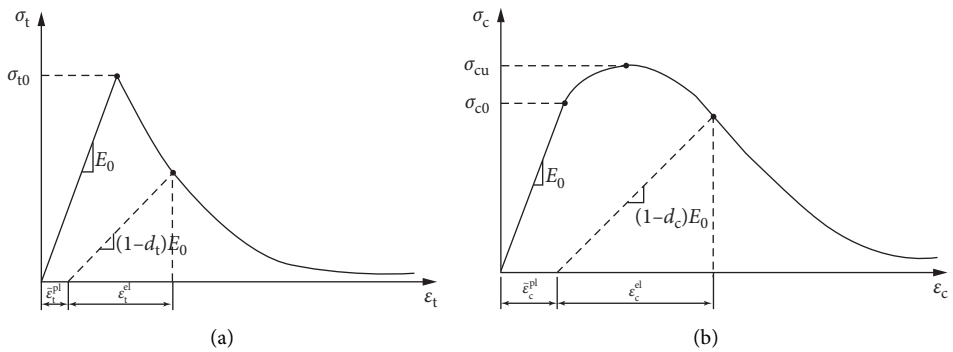

Figure 12: Stress-strain diagram of concrete damaged plasticity model. (a) Tension; (b) compression.

lower than the design value of concrete compressive strength.

The displacement time-history curve at characteristic point 5 at the top of the middle pipe is selected to show the displacement variation trend of the structure under seismic excitation as shown in Figure 10. The maximum displacement response is given in Table 4.

The displacement response time history at the characteristic point 5 on the top of the middle pipe was analyzed to study the overall displacement response of the structure. From Figure 10 and Table 4, it can be seen that the seismic displacement response under both conditions with water or not lags behind the time-history curves of artificial seismic wave displacement. This is because the seismic wave takes a

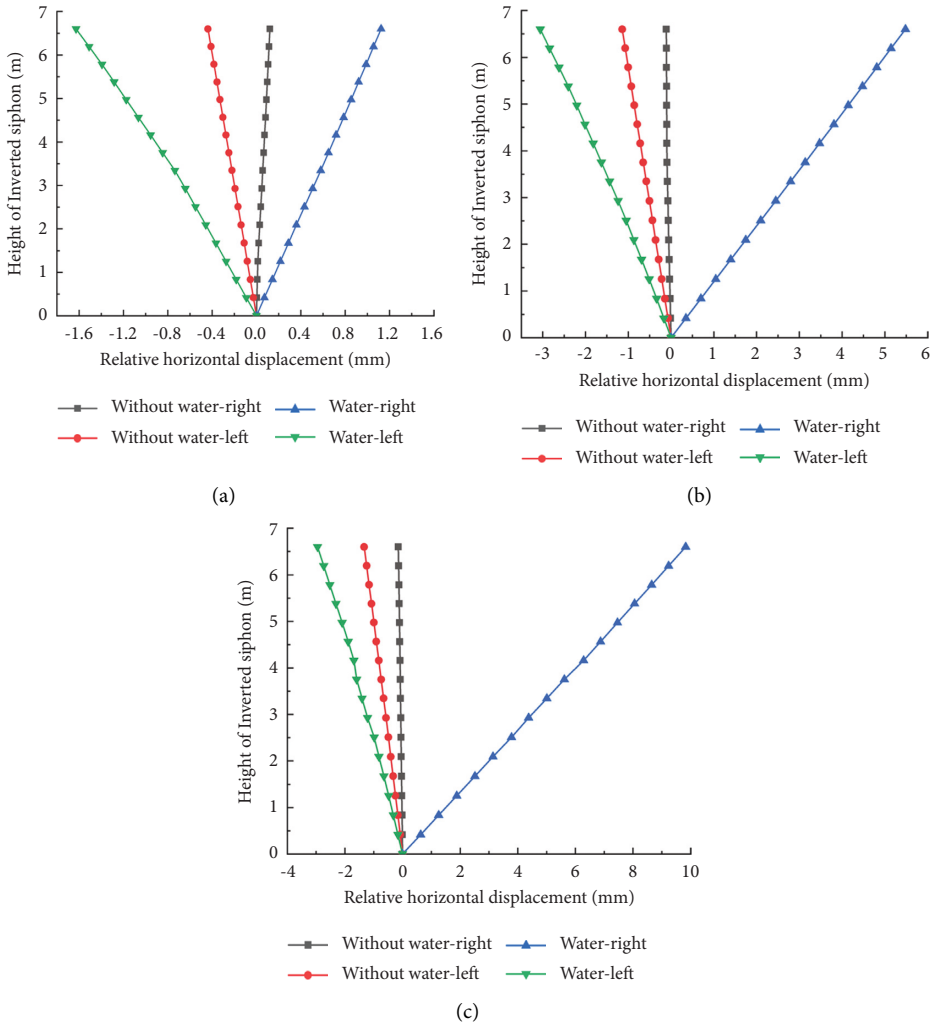

Figure 13: Variation curve of horizontal relative displacement along the height. (a) PGA 0.24 g; (b) PGA 0.36 g; (c) PGA 0.48 g.

certain period of time to pass from the bottom of the soil into the structure when the ground motion input by the visco-elastic boundary. The horizontal displacement response of the structure is approximately 1.5–2 times of the vertical displacement response, and the inverted siphon structure sways horizontally with earthquake. The change trend of the absolute displacement on characteristic point 5 is the same whatever water or not. However, the horizontal displacement response of the structure with water is significantly larger than that without water, and the largest increase was 28.57%.

The horizontal relative displacement of the inverted siphon structure is the horizontal displacement difference along the height relative to the pipe bottom. A path "P" is taken between feature points 7 and 8 as shown in Figure 9. The displacement of nodes on the path is extracted to obtain the curve of relative horizontal displacement along the height as shown in Figure 11.

From Figure 11, it is shown that the horizontal relative displacement value increases with the increase of height, which is more obvious in conditions with water than without water. The horizontal relative displacement curve of the pipe body is approximately symmetric without water. The relative displacement of the pipe body's left side is larger with water. The existence of water in the pipe increases the deformation of the structure.

Table 5: Envelope values of horizontal relative displacement of structure.

Working condition	Envelope values of horizontal relative displacement of structure/mm		
	0.24 g	0.36 g	0.48 g
Without water	0.56	1.03	1.48
Water	2.75	8.54	12.78

5. Damage Analysis of Structure

In order to study the damage law of inverted siphon structure, the concrete damaged plasticity model (CDP, shown in Figure 12) is used to simulate the concrete pipes of inverted siphon, and user-defined element is used to simulate the fluid-structure interaction. Three artificial seismic

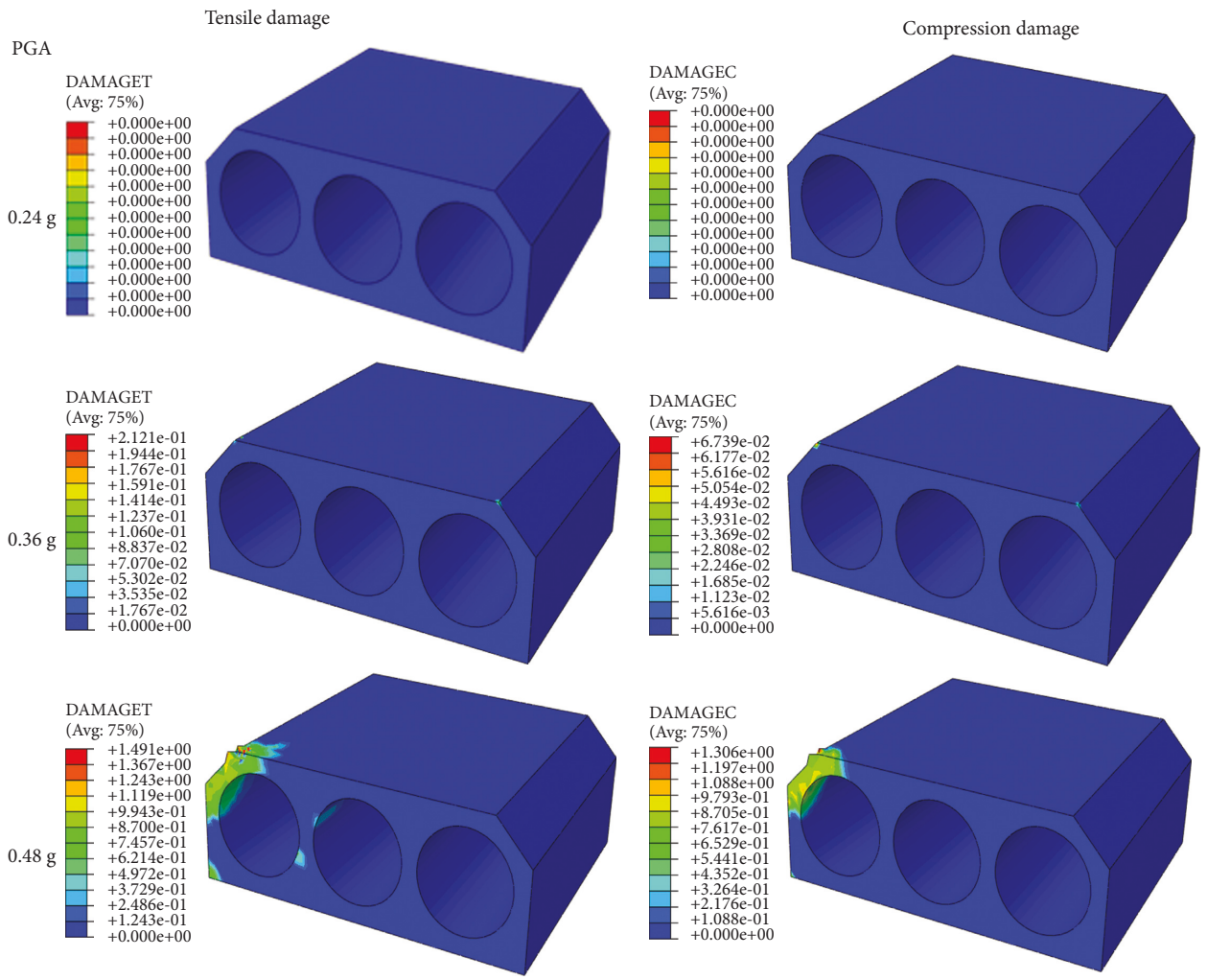

Figure 14: Nephogram of damage distribution of empty pipe condition.

waves with peak accelerations [15] (PGA) of 0.24 g, 0.36 g, and 0.48 g are input, respectively, for a duration of 20 seconds.

Under the different PGA values, the relative horizontal displacement of the structure along the height is shown in Figure 13.

The relative displacement envelope values of the inverted siphon structure are shown in Table 5.

From Figure 13 and Table 5, it can be seen that the horizontal relative displacement of the inverted siphon structure increases with the increase in PGA. However, the change of relative displacement is nonlinear with the change in PGA. With the same PGA, the relative horizontal displacement envelope values with water are significantly larger than that without water and about 5–8 times.

When PGA is 0.24 g, the horizontal sloshing amplitude of the pipe structure is basically symmetric. The deformation of the pipe structure is larger with the increase in PGA because a large internal damage has occurred.

In this paper, damage factors were used to characterize the damage degree of inverted siphon structure under earthquake action, and the distribution of damage factors of structure is shown in Figures 14 and 15.

At the empty pipe condition, the concrete pipes of the inverted siphon are not damaged when PGA is 0.24 g, and the concrete pipes are damaged at the corner point when PGA is 0.36 g. With the increase in PGA, the damage degree is intensified. When PGA is 0.48 g, the tensile and compression damage factors at the corner position are close to 1.0, and the concrete has been a failure as shown in Figure 14.

At the three pipes water-filled condition, the concrete pipes are damaged at the corner point when PGA is 0.24 g. When PGA is 0.36 g, the damage position is on the outer side of the inner wall of both sides and in the middle of the middle wall. When PGA is 0.48 g, there is a wide range of damage in both side wall and middle wall, the damage factors are close to 1.0, and the concrete is a failure in a large range as shown in Figure 15.

With water or not, the concrete pipes are first damaged at the corner, which conforms to the basic law of abnormal structure, and the damage area of tensile damage is generally larger than that of compression damage. With the increase in PGA, the damage area with water grows faster than that without water, and the damage area develops rapidly from the structure corner to the inside of the pipes. The

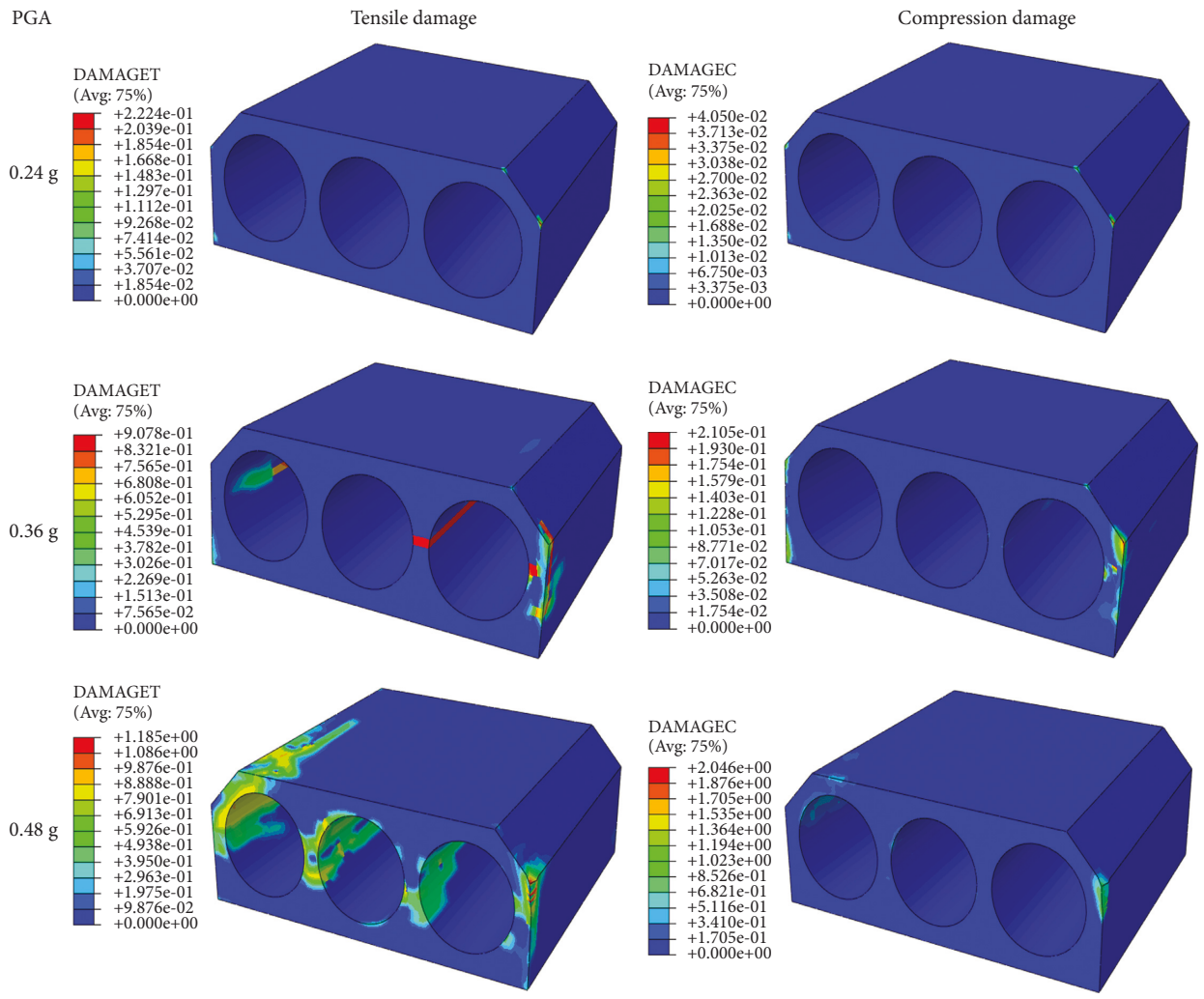

Figure 15: Nephogram of damage distribution of three pipes water-filled condition.

continuous development of damage leads to the final failure of the structure.

6. Conclusion

In this paper, the function of water is realized by user-defined element subprogram, and the dynamic response of Xiazhuang inverted siphon structure is calculated under three sets of seismic wave excitation, and the nonlinear damage analysis of the pipes is carried out by using concrete plastic damage element with different PGA. The results indicate the following:

(1) The horizontal displacement response of the pipes is larger than the vertical displacement response, which is mainly represented by the horizontal shaking with the action of earthquake, and it is easy to produce relative displacement in the horizontal direction and deviate from the initial position.

In order to reduce the influence of horizontal displacement under the action of earthquake, the gravel cushion should be appropriately thickened between the bottom of the pipe and the foundation.

(2) The existence of water in the pipes increases the dynamic response of the structure, and the horizontal relative displacement of the structure with water has a significant increase compared with that without water.

(3) With water or not, the concrete pipes are first damaged at the corner, which conforms to the basic law of abnormal structure, and the damage area of tensile damage is generally larger than that of compression damage.

(4) With the increase in PGA, the damage area with water grows faster than that without water, and the damage area grows rapidly from the structure corner to the inside of the pipes. The continuous development of damage leads to the final failure of the structure.

Data Availability

The data used to support the findings of this study are available from the corresponding author upon request.

Conflicts of Interest

The authors declare no conflicts of interest regarding the publication of this paper.

Acknowledgments

This research was funded by the National Natural Science Foundation of China (11502081), the Science and Technology Project of Henan Province (212102310951 and 192102310210), and the Foundation from MWR Center for Levee Safety and Disease Prevention Research (2019005 and LSDP202102).

References

[1] S. Zhao, X. Li, and Z. Hu, "Experimental study on simulated model of large prestressed concrete inverted siphon," *Journal of Hydroelectric Engineering*, vol. 25, no. 1, pp. 40–44, 2006.

[2] S. Liu, Y. Zhou, D. Zhang, J. Zhang, D. Zhang, and W. Ke, "Study on temperature control and crack prevention measures of circular-hole-square inverted siphon during construction period," *Journal of North China University of Water Resources and Electric Power (Natural Science Edition)*, vol. 41, no. 01, pp. 76–82, 2020.

[3] Y. Shi, D. Zhang, and D. Zhang, "Study on reasonable pipe section length of large inverted siphon," *Water Power*, vol. 47, no. 04, pp. 63–69+73, 2021.

[4] H. Wang, X. Li, and S. Zhao, "Dynamic response of large box-shaped inverted siphon under complex geological conditions," *Water Power*, vol. 37, no. 07, pp. 19–22, 2011.

[5] H. Wang, J. Wu, S. Sun et al., "Glucosinolate biosynthetic genes in Brassica rapa," *Gene*, vol. 487, no. 2, pp. 135–142, 2011.

[6] P. Xu, X. Tang, and T. Xia, "Analysis on earthquake response of the inverted siphon concrete pipes," *Northwestern Seismological Journal*, vol. 29, no. 04, pp. 352–356+376+294, 2007.

[7] X. Ai and J. Li, "Analysis of seismic response of underground pipelines in terms of effective stress," *Journal of Disaster Prevention and Mitigation Engineering*, vol. 25, no. 01, pp. l–7, 2005.

[8] D. Fu and Y. Gu, "Research on seismic response of mountain tunnel considering soil-structure dynamic interaction[J]," *Journal of Guangxi University(Natural Science Edition)*, vol. 44, no. 01, pp. 176–182, 2019.

[9] X. Han, L. Tao, C. Liu, S. An, and X. Wu, "Analysis of influencing factors of seismic response of connected parallel subway stations," *Journal of Beijing University of Technology*, vol. 46, no. 08, pp. 929–939, 2020.

[10] H.-L. Qu, H. Luo, H.-G. Hu, H.-Y. Jia, and D.-Y. Zhang, "Dynamic response of anchored sheet pile wall under ground motion: analytical model with experimental validation," *Soil Dynamics and Earthquake Engineering*, vol. 115, pp. 896–906, 2018.

[11] H.-l. Qu, Y.-y. Deng, Y.-n. Gao, X. Huang, and Z. Zhang, "Time history of seismic earth pressure response from gravity retaining wall based on energy dissipation," *Journal of Mountain Science*, vol. 19, no. 2, pp. 578–590, 2022.

[12] J. Liu, Z. Wang, and X. Du, "Three-dimensional visco-elastic artificial boundaries in time domain for wave motion problems," *Engineering Mechanics*, vol. 22, no. 06, pp. 46–51, 2005.

[13] GB 18306, "Seismic Ground Motion Parameter Zonation Map of China," 2015, https://www.researchgate.net/figure/Seismic-ground-motion-parameter-zonation-map-of-China_fig1_307642649.

[14] GB51247, "Standard for seismic design of hydraulic structures," 2018, https://www.publications.usace.army.mil/Portals/76/Publications/EngineerManuals/EM_1110-2-6053.pdf.

[15] G. L. Fenves, S. Mojtahedi, and R. B. Reimer, "Effect of contraction joints on earthquake response of an arch dam," *Journal of Structural Engineering*, vol. 118, no. 4, pp. 1039–1055, 1992.